Control Engineering Practice 76 (2018) 112–122

Contents lists available at ScienceDirect

Control Engineering Practice

journal homepage: www.elsevier.com/locate/conengprac

Modeling and control of unmanned aerial/underwater vehicles using hybrid control

Diego Alberto Mercado Ravell, Marco Moreno Maia, Francisco Javier Diez *

Department of Mechanical and Aerospace Engineering Rutgers, the State University of New Jersey, 98 Brett Road, Piscataway, NJ 08854-8058, United States

ARTICLE INFO

Keywords:
Multi-medium systems
Hybrid control
Unmanned aerial/underwater vehicles
Multirotors
Trajectory tracking

ABSTRACT

Modeling and control of a multi-medium unmanned vehicle capable of seamless operation in air or underwater is introduced in this paper. The multi-medium system is treated as a hybrid system with continuous dynamics while performing in both air and underwater, and discrete jumps in the medium density during the transitions. The continuous dynamics are modeled by the Newton–Euler formalism, taking into account the effects of the buoyancy and drag phenomena, normally neglected in aerial vehicles.

A hybrid controller is designed for trajectory tracking considering the full system, including a transition strategy to assure the switching between mediums. Stability analysis for the full system is provided using hybrid Lyapunov and invariance principles. The performance of the control strategy is validated through simulations. Finally, an experimental platform consisting of a multirotor in an octo-quadcopter configuration was developed and some preliminary experimental results are introduced, showing the vehicle performing in air, underwater and through the transition.

1. Introduction

Control of autonomous vehicles, or mobile robots, has attracted much attention all over the world in the last decades, due to their broad range of applications such as surveillance, inspection, fast delivery, search and rescue, among many others. The use of autonomous vehicles in a multi medium environment (ground, air or water) is a more recent topic and some examples can be found for ground/aerial or ground/underwater systems (Crespi, Karakasiliotis, Guignard, & Ijspeert, 2013). However, the development of aerial/underwater vehicles presents more challenges, mainly due to the drastic change in fluid density and viscosity between mediums which directly affects the dynamics of the system, the payload limitations in flight mode, the limitations of some sensors underwater (no GPS signals available), corrosion underwater, and the waterproof requirement on the whole vehicle, specially on the electronic components.

The idea of an entity that can fly and swim is not new though, and some examples of animals can be found in the nature such as flying fishes or aquatic birds. The first designs for air/underwater vehicles can be tracked back to the 1930's, when the Denmark Navy conceived a submarine plane (Unknown, 1930), and in the Soviet Union a flying underwater boat was proposed (Petrov, 1995), but they were never built. More recently, some designs of submersible airplanes have appeared with successful preliminary implementations (Edwards, 2014; Fabian, Feng, Swartz, Thurmer, & Wang, 2012), but they present complicated mechanics and are constrained to small depths. Others, such as Kollmorgen (2009) and Majumdar (2013), present UAVs (Unmanned Aerial Vehicles) that can be launched from underwater, but their underwater capabilities are very limited. Further related works include multirotors capable of floating on the water surface and deploying sensors underwater with a tether (Jones, Dobrokhodov, & Dillard, 2016), and quadrotor-like vehicles with only underwater capabilities (Ranganathan, Thondiyath, & Kumar, 2015; Tanaka, Fuji, Matsuo, & Takimoto, 2016).

On the other hand, the concept of hybrid control systems has been recently applied to UAVs (Alexis, Huerzeler, & Siegwart, 2014; Cassau, Sanfelice, Cunha, Cabecinhas, & Silvestre, 2015; Naldi, Furci, Sanfelice, & Marconi, 2013; Smith & Sanfelice, 2016). Here, the term "hybrid system" is understood in the sense of a system whose dynamics depend on a coupling between continuous and discrete variables (Goebel, Sanfelice, & Teel, 2012; van der Shaft & Schumacher, 2000). For example, in Smith and Sanfelice (2016) a waypoint transitioning and loitering hybrid control is designed for fixed wing UAVs. In Cassau et al. (2015) a hybrid quaternion feedback strategy is applied to a class of underactuated vehicles with a single force direction, such as multirotors and helicopters. The hybrid representation allows one to determine in

* Corresponding author.
E-mail address: diez@jove.rutgers.edu (F.J. Diez).

https://doi.org/10.1016/j.conengprac.2018.04.006
Received 5 November 2016; Received in revised form 9 April 2018; Accepted 11 April 2018
Available online 2 May 2018
0967-0661/

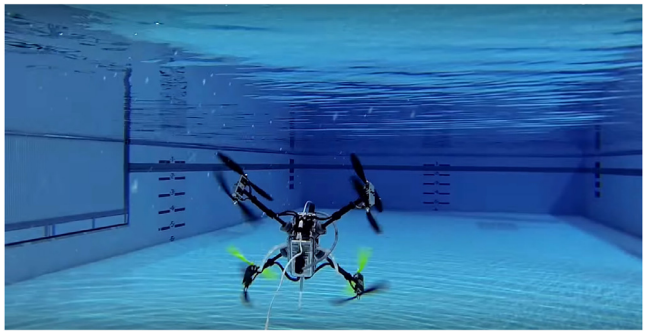

Fig. 1. Naviator NV03 on an underwater mission, former aerial/underwater prototype developed by Rutgers University, 2014.

a unique way the attitude of the vehicle. The use of a Hybrid system representation arises naturally for the case of multi-medium vehicles, where the change in the medium can be modeled as a discrete event, or in other words, a jump in the continuous dynamics.

This work deals with the modeling and control for autonomous navigation of the so called "Naviator" (Fig. 1), the first unmanned vehicle of its class to successfully merge together Unmanned Aerial Vehicles (UAVs) and Unmanned Underwater Vehicles (UUVs), combining their air and underwater capabilities (Maia, Soni, & Diez, 2015).

Due to their maneuverability, hover capability and simplified mechanics, a multirotor configuration has been chosen for this work. In particular, as a proof of concept, an octocopter in "X8" configuration was successfully developed and operated in air, underwater, and more importantly it demonstrated seamless transition between both mediums. The concept of modeling of an air/water multirotor vehicle has been recently described in Drews, Neto, and Campos (2014) and Neto, Mozelli, Drews, and Campos (2016), although no vehicle was built or tested. In Drews et al. (2014) linear Proportional Derivative (PD) controllers with compensation of the restoring forces are used for attitude stabilization and position control in simulations. Different gains are used for each medium. This work continuous in Neto et al. (2016) with the design of a robust attitude controller for a Linear Parameter Varying System (LPV), where the difference in the mediums density is considered as a time varying parameter. The conceptual design in Drews et al. (2014) and Neto et al. (2016) assumes the use of the upper four rotors exclusively for air and the bottom four only for water. In contrast, a multi-medium multirotor vehicle that uses all its rotors for both mediums (air and water) is considered in this paper, increasing the thrust force and eliminating the extra payload of unused motors for a particular medium. The presented vehicle is modeled as a hybrid system, where the change of medium is considered as a discrete event, rather than a time varying parameter. This allows to switch between different control laws depending on the operation mode, in particular on the transitions between media. Furthermore, real-time preliminary results are provided using a fully operational multi-medium multirotor vehicle. The proposed approach consists then in the design of a hybrid controller to acknowledge trajectory tracking for the full system. First, a trajectory tracking control is proposed for the case of only one medium (constant density). A hierarchical control based in a time scale separation of the translational and rotational dynamics is employed. This is possible since the rotational dynamics are much faster than the translational ones (Bertrand, Guénard, Hamel, Piet-Lahanier, & Eck, 2011). A feedback linearization strategy is chosen for the position control, using the reference angles as virtual control inputs. A PID (Proportional, Integral, Derivative) controller is used for the attitude control. The main difference with other controllers available for UAVs is the inclusion of the drag and buoyancy forces, usually ignored, but crucial for large medium density, as is the case underwater. The next step consisted in designing a transition strategy that ensures the switch between mediums without chattering. Finally, the full system is merged together as a closed-loop hybrid system.

The main contributions of this work can be summarized in the following points:

- The full model of the system will be proposed using the hybrid systems theory, where the abrupt change of density will be considered as a discrete time event.
- A control strategy for the trajectory tracking problem of the hybrid system will be designed, including a transition strategy to assure the switching between mediums without chattering. Furthermore, the stability of the full closed-loop system will be analyzed using hybrid Lyapunov theory and hybrid invariance principle, including the stability analysis during the transition.
- Finally, as a proof of concept, preliminary real-time experimental results will be provided for the first time for a multirotor unmanned multi-medium vehicle in semi-autonomous operation.

The remainder of the paper is organized as follows. The dynamical model is provided in Section 2 for the multi-medium vehicle represented as a hybrid system. In Section 3, a control strategy for the full system is proposed. The validity of the control strategy is tested in numerical simulations in Section 4. A fully operational prototype is described in Section 5, while some preliminary experimental results are presented in Section 6. Finally, conclusions and perspectives are discussed in Section 7.

2. Dynamical modeling

Multi-medium vehicles can be modeled as hybrid systems, where two different continuous systems define the dynamics of the vehicle depending on the environment (air or water), with discrete events representing the switching from one continuous state to the other.

In the air mode (altitude $z > 0$), the vehicle behaves as an UAV. Once the altitude decreases below certain small gap ϵ, a transition takes place. If the vehicle is completely underwater, it behaves as an UUV. Note that more than one transition state can be defined depending on the strategy used to perform the transition (decelerating some motors while accelerating others), and whether the vehicle is entering or exiting the water.

2.1. Rigid object immersed in a fluid

Modeling of aerial and underwater vehicles have been widely studied in the literature as separate systems (Fossen, 1994; Roskam, 1982). Both models attempt to describe a rigid object in a three dimensional space evolving in a fluid medium. The main difference between both systems relies in the change in medium density (three orders of magnitude difference). The effect of a larger density impacts in three main simplifications normally made for air vehicles that cannot be neglected underwater. They are the drag force, buoyancy force and added mass.

The drag force F_D is a resistive force acting opposite to the motion of the vehicle with respect to the surrounding fluid, and can be expressed for the unidimensional case as

$$F_D := \frac{1}{2} C_D A \rho v |v| \tag{1}$$

for a density ρ, characteristic area A, drag coefficient C_D and relative speed v between the object and the fluid. Note that this kind of force acts as a natural damper to the motions on a fluid. The drag coefficient depends on the geometry of the body, the vehicle's surface roughness and the Reynolds number R_e

$$R_e := \frac{vD}{\nu} \tag{2}$$

for a kinematic viscosity ν and a characteristic diameter D.

The buoyancy F_B is a restoring force exerted by a fluid, opposite to the gravity g of an immersed object. Its magnitude is equal to the

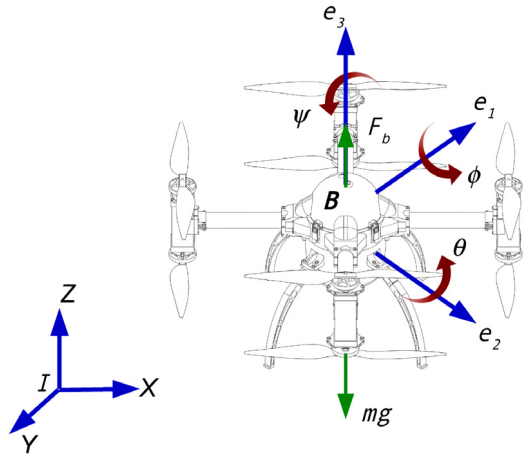

Fig. 2. Unmanned aerial/underwater vehicle reference frames.

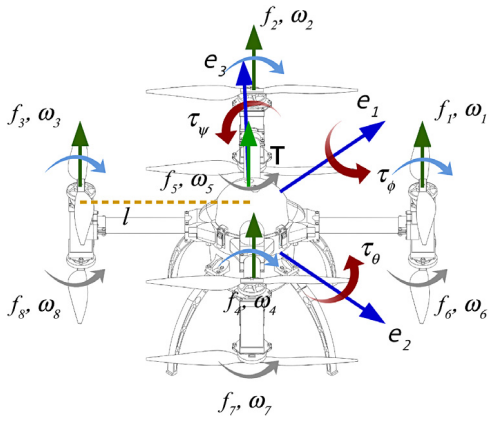

Fig. 3. Forces and moments on the air/underwater vehicle.

weight of the fluid displaced by the object. For an object with volume V the magnitude of the buoyancy is given by

$$F_B := \rho V g. \tag{3}$$

Underwater vehicles are normally designed to take advantage of the buoyancy force to compensate for the weight of the vehicle and be near neutrally buoyant ($weight \approx F_B$). Due to security constraints, underwater vehicles are usually slightly positively buoyant ($weight < F_B$) such that the vehicle will naturally return to the surface in case of any malfunction, allowing for an easy recovery.

Another phenomena called added mass arises since a rigid body immersed in a fluid should not only displace its own mass, but also the mass of the fluid surrounding it. The concept of added mass comprises pressure induced forces and moments, proportional to the acceleration of the vehicle. To get a sense of added mass and inertia for this vehicle, it can be estimated by approximating its main pressure vessel by a sphere. The added mass m_a for a sphere with radius r_v can be calculated as

$$m_a \approx \frac{2}{3}\pi\rho r_v^3. \tag{4}$$

Moreover, the added moment of inertia J_a for a thin spherical shell is given by

$$J_a \approx \frac{2}{3} m_a r_v^2 \tag{5}$$

along each axis. For the present vehicle, m_a and J_a were around one to two orders of magnitude smaller than the mass of the vehicle m and its moments of inertia. Given that the accelerations remain small for the present work, the added mass is negligible and not modeled.

2.2. Dynamic model for a constant density medium

Define an inertial frame fixed to the ground **I**, and a body fixed frame **B**, as depicted in Fig. 2. Then, the dynamic model of the unmanned aerial/underwater vehicle, with mass m and inertia matrix $\mathbf{J} \in \mathbb{R}^{3\times3}$, can be obtained by the Newton–Euler equations as (see for example Castillo, Lozano, & Dzul, 2005; Hamel, Mahony, Lozano, & Ostrowsky, 2002):

$$\dot{\boldsymbol{\xi}}_\mathbf{1} = \boldsymbol{\xi}_\mathbf{2} \tag{6}$$

$$m\dot{\boldsymbol{\xi}}_\mathbf{2} = T\mathbf{R}\mathbf{e_3} - g(m - \rho V)\mathbf{e_3} - \mathbf{C}_{\mathbf{D}_\xi}\rho\mathbf{D}_\xi\xi_2 + m\xi_2 \times \boldsymbol{\Phi}_2 \tag{7}$$

$$\dot{\boldsymbol{\Phi}}_1 = \mathbf{Q}^{-1}\boldsymbol{\Phi}_2 \tag{8}$$

$$\mathbf{J}\dot{\boldsymbol{\Phi}}_2 = \Gamma - \boldsymbol{\Phi}_2 \times \mathbf{J}\boldsymbol{\Phi}_2 - \mathbf{C}_{\mathbf{D}_\phi}\rho\mathbf{D}_\phi\boldsymbol{\Phi}_2 \tag{9}$$

where $\boldsymbol{\xi}_\mathbf{1} \in \mathbb{R}^3 := [x\ y\ z]^T$, $\boldsymbol{\xi}_\mathbf{2} \in \mathbb{R}^3$ are the linear position and velocity vectors with respect to the inertial frame **I**, $\boldsymbol{\Phi}_1 := [\phi\ \theta\ \psi]^T$ denotes the Euler angles roll, pitch respectively yaw. The body fixed angular speed is given by $\boldsymbol{\Phi}_2 \in \mathbb{R}^3$. g is the gravity constant, $\mathbf{R}(\boldsymbol{\Phi}_1) \in SO(3) : \mathbf{B} \to \mathbf{I}$ is a rotation matrix from the body fixed frame to the inertial one, and $\mathbf{e_3} := [0\ 0\ 1]^T$. $\mathbf{Q}^{-1}(\boldsymbol{\Phi}_1) \in \mathbb{R}^{3\times3}$ is a transformation matrix between the body fixed angular rate and the Euler angles rate. The matrices $\mathbf{D_i}$ are diagonal with absolute value elements, i.e. $\mathbf{D}_\xi := diag\{|\dot{x}|\ |\dot{y}|\ |\dot{z}|\}$, $\mathbf{D}_\phi := diag\{|\dot{\phi}|\ |\dot{\theta}|\ |\dot{\psi}|\} \in \mathbb{R}^3$. $\mathbf{C}_{\mathbf{D}_\xi}(\mathbf{R_e})$, $\mathbf{C}_{\mathbf{D}_\phi}(\mathbf{R_e}) \in \mathbb{R}^{3\times3}$ are the diagonal drag coefficient matrices which depend on the Reynolds number $\mathbf{R_e}$ and the geometry of the vehicle, particularly on the cross-sectional area A. Further discussions about the drag coefficients can be found in Kundu and Cohen (2008). V stands for the volume of the vehicle. The medium density is denoted by $\rho \in \{\rho_A,\ \rho_W\}$, with air density $\rho_A \approx 1.2754\ \mathrm{kg/m^3}$, and water density $\rho_W \approx 1000\ \mathrm{kg/m^3}$. Finally, the Coriolis force $m\xi_2 \times \boldsymbol{\Phi}_2$ is usually small unless aggressive maneuvers are considered.

For the particular case of a multirotor in an octo-quadcopter configuration, the input vector is given by $\mathbf{u} \in \mathbb{R}^4 := [T\ \Gamma]^T$, with the total thrust $T := \sum_{i=1}^{8} f_i$, and the torques $\Gamma \in \mathbb{R}^3$ generated from the forces f_i produced by the eight rotors in the following manner

$$\mathbf{u} = \begin{bmatrix} 1 & 1 & 1 & 1 & 1 & 1 & 1 & 1 \\ -l & l & l & -l & l & -l & -l & l \\ l & l & -l & -l & l & l & -l & -l \\ -b & b & -b & b & b & -b & b & -b \end{bmatrix} \mathbf{f} \tag{10}$$

$$\mathbf{f} := \boldsymbol{\omega}^T\boldsymbol{\omega}\rho K_m \tag{11}$$

where l is the distance from the rotor center to the center of mass of the vehicle and b is a constant that maps the rotational speed of each motor to its torque. The rotors force vector $\mathbf{f} \in \mathbb{R}^8 := [f_1\ \dots\ f_8]^T$ is proportional to the medium density ρ, the quadratic of the motor's speed vector $\boldsymbol{\omega} \in \mathbb{R}^8 := [\omega_1\ \dots\ \omega_8]^T$ and the motor's constant K_m. As depicted in Fig. 3, four rotors spin clockwise and four spin counter-clockwise in order to cancel the reactive torques, considerably simplifying the dynamics of the system.

2.3. Hybrid system model

Unmanned multi-medium systems can be seen as hybrid systems where the dynamics evolve continuously along time until a change of medium occurs as a discrete event. When that happens, the density ρ jumps aggressively from one value to another. In this case, the jump occurs when the altitude z reaches the water level, i.e. $z = 0$. More precisely, a transition zone can be defined where the vehicle is partially in both mediums at the same time, hence the density is somewhere in between the extreme values $\rho \in (\rho_A, \rho_W)$. Defining $\epsilon \in \mathbb{R}^+$ as the gap

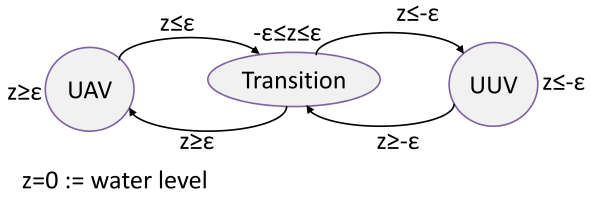

Fig. 4. Unmanned multi-medium vehicle modeled as a hybrid automata.

where such transition occurs, the system can be modeled as a hybrid automata as depicted in Fig. 4.

In this work, the definition of a hybrid system proposed by Goebel et al. (2012) is adopted. A hybrid system $\mathscr{H}$ with hybrid time domain $(t, j) \in \mathbb{R}^+ \times \mathbb{N}$, where t is the continuous time and j are the jump times, is defined by the data $\mathscr{H} = (F, C, G, D)$, composed by a state space $O \subset \mathbb{R}^n$ where the state η is restricted, a flow map $F : O \rightrightarrows \mathbb{R}^n$ describing the continuous behavior of the system, a flow set $C \subset O$ specifying when the continuous evolutions can occur, a jump map $G : O \rightrightarrows O$ which determines the value of the state after a jump, denoted by $\eta^+ \in G(\eta)$, and a jump set $D \subset O$ where the discrete jumps may occur. The hybrid system $\mathscr{H}$ can then be represented as

$$\mathscr{H} : \begin{cases} \dot{\eta} \in F(\eta) & \eta \in C \\ \eta^+ \in G(\eta) & \eta \in D. \end{cases} \tag{12}$$

For the particular case of a vehicle evolving in two different mediums, the state may be defined as $\eta \in O := [\boldsymbol{\xi_1}\ \boldsymbol{\xi_2}\ \boldsymbol{\Phi}_1\ \boldsymbol{\Phi}_2\ \rho]^T$ with the space state given by $O := \mathbb{R}^{12} \times \{\rho_A, \rho_W\}$. Note the inclusion of the density ρ as an additional state. The set-valued map $F(\eta)$ is obtained stacking together Eqs. (6)–(9) with $\{0\}$ (the density ρ remains constant during continuous flows). Continuous evolutions, also referred as flows, are allowed only within the flow set $C := O$. Jumps occur when the altitude reaches the water level ($z = 0$), hence the jump set is defined as $D := \{\eta \mid z = 0\}$ and the jump map takes the form

$$G(\eta) := \left\{ \left[\xi_1\ \xi_2\ \boldsymbol{\Phi}_1\ \boldsymbol{\Phi}_2\ \{\rho_A, \rho_W\}\right]^T \quad \eta \in D. \right. \tag{13}$$

Note that in reality the change of density does not go from one value to the other instantly, but there exist a zone where the body is partially submerged underwater and partially in air ($|z| \leq \epsilon$, with ϵ equal to the height of the vehicle), such that the density takes values somewhere within the interval $\rho = (\rho_A, \rho_w)$. This issue will be considered in the design of the control strategy for the hybrid system in Section 3.3.

For further details on the dynamical modeling, the interested reader is referred to Fossen (1994) for the case of underwater vehicles, and to Roskam (1982) for aerial vehicles.

3. Control strategy

Consider the problem of trajectory tracking for a multi-medium vehicle represented as a hybrid system with continuous evolution given by Eqs. (6)–(9) and discrete jumps (13). Before proceeding to the design of the controller, let the desired trajectory be $\eta_d(t)$ and the tracking error be $\bar{\eta} = [\bar{\xi}_1\ \bar{\xi}_2\ \bar{\Phi}_1\ \bar{\Phi}_2\ \rho]^T := \eta - \eta_d$.

The vehicle under consideration is an under actuated system with four inputs and six outputs. To solve it, the problem is partitioned in three sub-problems. The first part consists in designing a control law for the case when the vehicle performs exclusively in one medium, and the density remains constant. The considered approach is a hierarchical controller based in a time scale separation between the translational and rotational dynamics. This is possible since the rotations are much faster than the translations. In this manner, the position ξ_1 can be controlled using the desired angles as virtual control inputs. A second controller in cascade can be designed for the attitude stabilization to a desired reference ($\lim_{t\to\infty} \boldsymbol{\Phi}_1 \to \boldsymbol{\Phi}_{1_d}$). This work focuses on the study of the translational dynamics, assuming that the rotational ones rapidly stabilize to their desired reference. The second sub-problem consist in the design of a transition strategy that warranties the change between media. Finally, a hybrid control is developed for the full multi-medium system, including a transition strategy. The block diagram of the overall control strategy can be seen in Fig. 5.

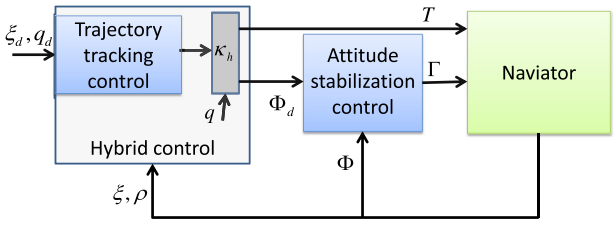

Fig. 5. Block diagram of the control strategy. Three levels of control are used, a hybrid controller to switch according to the operation mode, a trajectory tracking control and an attitude stabilization control.

3.1. Trajectory tracking for a single medium

Problem 1 (*Trajectory Tracking with Constant Density*)**.** Design a control law $\mathbf{u} = \kappa_s(\eta)$ such that, for a constant density ρ, the system (6)–(9) converges asymptotically to a desired reference η_d, i.e. $\lim_{t\to\infty} \eta = \eta_d$

Consider the following position error dynamics with the new virtual control input $\nu := T\mathbf{R}(\boldsymbol{\Phi}_{1_d})\mathbf{e_3}$

$$\mathbf{F}_\xi := \begin{cases} \dot{\bar{\xi}}_1 = \bar{\xi}_2 \\ m\dot{\bar{\xi}}_2 = \nu - g(m - \rho V)\mathbf{e_3} - \mathbf{C}_{\mathbf{D}_\xi}\rho\mathbf{D}_\xi\xi_2 + m\xi_2 \times \boldsymbol{\Phi}_2 - m\dot{\xi}_{2_\mathbf{d}} \end{cases} \tag{14}$$

where the bar on top of the variables represents the errors between the real states and the desired ones, denoted by the "d" subscript.

Lemma 1. *The following feedback linearization control law ν_s renders the system (14) asymptotically stable for some diagonal and positive definite constant gain matrices $\mathbf{K}_{\mathbf{p}_\xi}$, $\mathbf{K}_{\mathbf{d}_\xi} \in \mathbb{R}^{3\times3}$.*

$$\nu_s = g(m - \rho V)\mathbf{e_3} + \mathbf{C}_{\mathbf{D}_\xi}\rho\mathbf{D}_{\xi_2}\xi_2 - m\xi_2 \times \boldsymbol{\Phi}_2 + m\dot{\xi}_{2_\mathbf{d}} - \mathbf{K}_{\mathbf{p}_\xi}\bar{\xi}_1 - \mathbf{K}_{\mathbf{d}_\xi}\bar{\xi}_2. \tag{15}$$

Proof. Define $\bar{\xi}_3 := \bar{\xi}_1 + \mathbf{K}_1^{-1}\bar{\xi}_2$ and consider the Lyapunov candidate function $V_1 : [0, \infty) \times \mathbb{R}^6 \to \mathbb{R}$, with a diagonal and positive definite matrix $\mathbf{K_1}$

$$V_1 = \frac{1}{2}\bar{\xi}_1^T\bar{\xi}_1 + \frac{1}{2}\bar{\xi}_3^T\bar{\xi}_3 \tag{16}$$

the time derivative is given by

$$\begin{aligned} \dot{V}_1 = & -\bar{\xi}_1^T\mathbf{K_1}\bar{\xi}_1 + \bar{\xi}_3^T\mathbf{K_1}\bar{\xi}_3 + \frac{1}{m}\bar{\xi}_3^T\mathbf{K}_1^{-1} \\ & (\nu - g(m - \rho V)\mathbf{e_3} - \mathbf{C}_{\mathbf{D}_\xi}\rho\mathbf{D}_\xi\xi_2 + m\xi_2 \times \boldsymbol{\Phi}_2 - m\dot{\xi}_{2_\mathbf{d}}) \end{aligned} \tag{17}$$

applying the control law (15)

$$\begin{aligned} \dot{V}_1 = & -\bar{\xi}_1^T\mathbf{K_1}\bar{\xi}_1 + \bar{\xi}_3^T\mathbf{K_1}\bar{\xi}_3 \\ & + \frac{1}{m}\bar{\xi}_3^T\mathbf{K}_1^{-1}(-\mathbf{K}_{\mathbf{p}_\xi}\bar{\xi}_1 - \mathbf{K}_{\mathbf{d}_\xi}\bar{\xi}_2) \end{aligned} \tag{18}$$

choosing $\mathbf{K}_{\mathbf{p}_\xi} = m(\mathbf{K}_1^2 + \mathbf{K_1}\mathbf{K_2})$ and $\mathbf{K}_{\mathbf{d}_\xi} = m(\mathbf{K_1} + \mathbf{K_2})$, for any diagonal and positive definite constant matrix $\mathbf{K_2}$, yields

$$\dot{V}_1 = -\bar{\xi}_1^T\mathbf{K_1}\bar{\xi}_1 - \bar{\xi}_3^T\mathbf{K_2}\bar{\xi}_3 < 0. \quad \square \tag{19}$$

The control law and the proof are close to the ones presented in Hamel et al. (2002), with the addition of the drag and buoyancy forces.

For the attitude control, it is proposed a linear PID controller with drag compensation of the form

$$\Gamma = -\mathbf{K}_{\mathbf{p}_\phi}(\boldsymbol{\Phi}_1 - \boldsymbol{\Phi}_{1_d}) - (\mathbf{K}_{\mathbf{d}_\phi} - \mathbf{C}_{\mathbf{D}_\phi}\rho\mathbf{D}_\phi)\boldsymbol{\Phi}_2. \tag{20}$$

Finally the control law for the case of a constant medium density is given by

$$\boldsymbol{\kappa_s} := [\|v_s\| \ \Gamma]^T. \tag{21}$$

It is interesting to notice that the attitude stabilization underwater is not as crucial as in air. On air mode orientations far away from the origin will result in fast accelerations on the vehicle, and may cause it to fall and crash. Meanwhile, underwater operation allows safe operation in any orientation thanks to the near neutral buoyancy of the vehicle, normally selected by design to compensate for weight, and the increased drag when compared to air.

There exist a wide variety of control techniques in the literature for multirotors on a constant medium, specially in air (to cite some examples Hamel et al., 2002; Kendoul, Lara, Fantoni, & Lozano, 2006; Mercado, Castillo, Castro, & Lozano, 2014). Any other available strategy can be used as long as it is adapted to take into account the effects of the drag and buoyancy forces. Normally they are negligible for aerial vehicles due to its minor contribution, but for high density values, such as for underwater applications, these forces increase considerably. Assuming that the volume of the vehicle V and fluid density are constant, the buoyancy remains constant as well and is easy to compensate for. As for the drag force, it helps damping the movements. In the design of the controller, this results in lower derivative gains required (and bigger proportional ones) to obtain a good response for larger medium densities.

3.2. Transition control

Problem 2 (*Medium Transition Strategy*). Design a control strategy $\mathbf{u} = \boldsymbol{\kappa_t}$ for the error system (14), such that for a constant gap $\epsilon_2 \geq \epsilon_1 \in \mathbb{R}^+$ arbitrarily close to the medium boundary, every system trajectory entering the transition zone $|z| \leq \epsilon_2$ will abandon it after one and only one change of medium, while the rest of the system remains stable.

Intuitively, the vehicle can be designed to be heavier than buoyant ($m > \rho V$), i.e. negatively buoyant, in order to descend if no other force is applied. Then, just turning-off the motors will be enough to enter into the water. Note that, with the selected configuration, weight is the only negative component of the force in the vertical axis. On the other hand, on the transition the top rotors will be in air while the bottom ones will remain underwater, then, speeding up the top motors to obtain their maximum thrust $\frac{1}{2}T_{max}$ or a nominal value such that the total thrust is greater than the restoring forces ($T_n > \max_{\rho\in\{\rho_A,\rho_W\}}(m - \rho V)$) will be enough to get out of the water. According to this idea, consider the following transition control law

$$\boldsymbol{\kappa_t} := [\|\boldsymbol{\nu_t}\| \ \Gamma]^T \tag{22}$$

where

$$\boldsymbol{\nu_t} := \varphi(\bar{\xi}_3)\mathbf{e_3} - m\mathbf{K_2}\bar{\xi}_3 + \mathbf{C}_{\mathbf{D}_\xi}\rho\mathbf{D}_{\xi_2}\xi_2 - m\xi_2 \times \Phi_2 + m\dot{\xi}_{2_\mathbf{d}} \tag{23}$$

with

$$\varphi(\bar{\xi}_3) := \begin{cases} 0 & \bar{\xi}_3^{\mathbf{T}}\mathbf{e_3} > 0 \\ T_n & \bar{\xi}_3^{\mathbf{T}}\mathbf{e_3} < 0. \end{cases} \tag{24}$$

Analyzing again the candidate Lyapunov function (16), the time derivative applying the transition control law (23) takes the form

$$\dot{V}_1 = -\bar{\xi}_1^T\mathbf{K_1}\bar{\xi}_1 + \frac{1}{m}\bar{\xi}_3^T\mathbf{K_1^{-1}}\mathbf{e_3}(\varphi(\bar{\xi}_3) - g(m - \rho V)) \tag{25}$$

since $\mathbf{K_1^{-1}}$ is diagonal and $\mathbf{e_3} := [0\ 0\ 1]^T$, it follows

$$\dot{V}_1 = \begin{cases} -\bar{\xi}_1^T\mathbf{K_1}\bar{\xi}_1 - \frac{g}{m}\mathbf{e_3}^T\mathbf{K_1^{-1}}\mathbf{e_3}(m - \rho V)\bar{\xi}_3^{\mathbf{T}}\mathbf{e_3} & \bar{\xi}_3^{\mathbf{T}}\mathbf{e_3} > 0 \\ -\bar{\xi}_1^T\mathbf{K_1}\bar{\xi}_1 + \frac{1}{m}\mathbf{e_3}^T\mathbf{K_1^{-1}}\mathbf{e_3}(T_n - g(m - \rho V))\bar{\xi}_3^{\mathbf{T}}\mathbf{e_3} & \bar{\xi}_3^{\mathbf{T}}\mathbf{e_3} < 0 \end{cases} \tag{26}$$

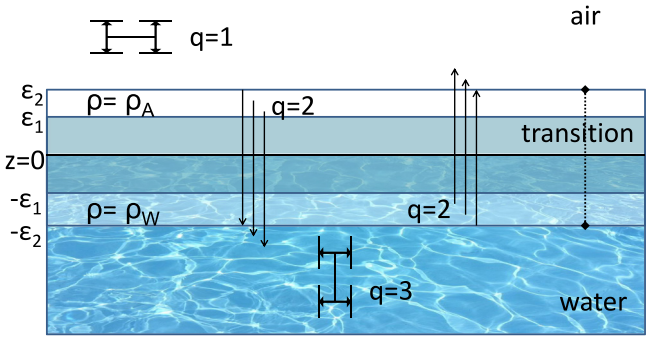

Fig. 6. Operation modes q according to the vehicle's altitude. q_1 and q_3 are respectively the air and underwater modes, while q_2 is the transition mode.

by choosing $T_n > \max_{\rho\in\{\rho_A,\rho_W\}}(m - \rho V)$ and $m > \rho V$, yields

$$\dot{V}_1 \leq 0 \tag{27}$$

and the system is stable at the transition, but is asymptotically stable for the z coordinate. Note that the largest set where $\dot{V}_1 = 0$ is given by $\{\bar{\xi}|\bar{\xi}_1 = 0, \bar{\xi}_2^{\mathbf{T}}\mathbf{e_3} = 0\}$.

Observe that in order to generate enough thrust to meet the nominal thrust condition ($T_n > \max_{\rho\in\{\rho_A,\rho_W\}}(m - \rho V)$) during the transitions water-to-air, it is required for the top rotors to be completely in air and to be powerful enough to produce the nominal thrust T_n. It is also interesting to observe the negative buoyancy requirement ($m > \rho V$) during transitions from air to water and for submersion, in contrast to the classical selection of positive buoyancy for underwater vehicles. This is necessary for the present configuration in order to have a negative force component in the vertical axis.

3.3. Hybrid controller for the full dynamic system

Problem 3 (*Closed-loop Hybrid Controller*). Design a closed-loop hybrid system $\mathscr{H}_c = (F_c, C_c, G_c, D_c)$ with a hybrid controller $\mathbf{u} = \boldsymbol{\kappa_h}$ for a multi-medium vehicle system (6)–(9) with variable medium density $\rho \in \{\rho_A, \rho_W\}$, such that given a desired reference η_d, the trajectory tracking error $\eta - \eta_d$ is globally asymptotically stable in spite of the change of medium density.

For the closed-loop hybrid system $\mathscr{H}_c = (F_c, C_c, G_c, D_c)$, let $q \in \{1, 2, 3\}$ be a discrete logic variable which determines the current operation mode (as depicted in Fig. 6, $q = 1$: air mode, $q = 2$: transition mode, $q = 3$: water mode). The state of the closed-loop system is defined as $\boldsymbol{\eta_c} := [\bar{\eta}\ q]^T$. The closed-loop flow map takes the form

$$\dot{\boldsymbol{\eta}}_\mathbf{c} \in \mathbf{F_c} := \begin{cases} \mathbf{F}_\xi \\ \mathbf{F}_\phi \\ [0, 0]^T \end{cases} \quad \boldsymbol{\eta_c} \in C_c \tag{28}$$

for $C_c := \mathbb{R}^{12} \times \{\rho_A, \rho_W\} \times \{1, 2, 3\}$, $\mathbf{F}_\xi$ as in Eq. (14) and $\mathbf{F}_\phi$ given by Eqs. (8), (9).

As previously stated, the change in density does not occur immediately for the entire vehicle, but there exists a transition zone where the system is partially on each medium ($|z| \leq \epsilon_1$), and the density is somewhere within the interval $\rho = (\rho_A, \rho_W)$. Furthermore, in order to assure a good transition between the mediums, a transition zone is defined such as $|z| \leq \epsilon_2$, with $\epsilon_2 \geq \epsilon_1 \geq 0$. In this zone, a transition strategy will govern the system's behavior. This second zone also allows to introduce hysteresis to the closed-loop system and avoid chattering. Then, four jumps are allowed:

– The vehicle enters the transition zone.

$$D_1 := \{\eta \mid |z| \leq \epsilon_2,\ q \neq 2\}.$$

– The vehicle exits the transition zone.

$$D_2 := \{\eta \mid |z| \geq \epsilon_2,\ q \neq (2 - \frac{z}{|z|})\}.$$

– Density change from air to water completed.

$$D_3 := \{\eta \mid z \leq -\epsilon_1,\ \rho = \rho_A\}.$$

– Density change from water to air completed.

$$D_4 := \{\eta \mid z \geq \epsilon_1,\ \rho = \rho_W\}.$$

The jump set is defined as $D_c := \cup_{i=1}^{4} D_i$, and the set-valued jump map G_c is given by

$$\eta_c^+ \in G_c(\eta) := \begin{cases} \begin{bmatrix}\xi_1 & \xi_2 & \Phi_1 & \Phi_2 & \rho & 2\end{bmatrix}^T & \eta \in D_1 \\ \begin{bmatrix}\xi_1 & \xi_2 & \Phi_1 & \Phi_2 & \rho & (2 - \frac{z}{|z|})\end{bmatrix}^T & \eta \in D_2 \\ \begin{bmatrix}\xi_1 & \xi_2 & \Phi_1 & \Phi_2 & \rho_W & q\end{bmatrix}^T & \eta \in D_3 \\ \begin{bmatrix}\xi_1 & \xi_2 & \Phi_1 & \Phi_2 & \rho_A & q\end{bmatrix}^T & \eta \in D_4. \end{cases} \tag{29}$$

Note that with this selection of the jump set and jump map, the discrete variables will be congruent with their physical meaning after at most one jump. Furthermore, the system is robust against arbitrary small perturbations in the neighborhood of the jump set.

A hybrid controller $\mathbf{u} = \boldsymbol{\kappa_h}(\bar{\eta}) \times q \in \mathbb{R}^4$ can be proposed, composed by a continuous part $\boldsymbol{\kappa_h}(\bar{\eta}) \times \{1, 3\} = \boldsymbol{\kappa_s}$ that renders the system stable for a constant density (see Lemma 1), and a transition controller to take the vehicle out of the transition zone (for example (22)). Henceforth, the hybrid control law takes the form

$$\boldsymbol{\kappa_h}(\bar{\boldsymbol{\eta}}, q) = \begin{cases} \boldsymbol{\kappa_s} & q \neq 2 \\ \boldsymbol{\kappa_t} & q = 2. \end{cases} \tag{30}$$

Observe that, by design, any solution entering the transition zone or starting at it cannot remain in an arbitrarily small neighborhood, but will exit it on the opposite boundary. For this reason, the additional condition $q_d \neq 2$, $|z_d| > \epsilon_2$ is imposed to the desired trajectory, such that $\bar{z} \neq 0$ in the transition. Under this condition, it can be shown that the hybrid closed-loop system (28), (29), with a hybrid control (30) is asymptotically stable. First, it can be observed that the hybrid system (28), (29) satisfies the hybrid basic conditions as defined in Goebel et al. (2012), i.e. the state space $O_c = \mathbb{R}^{12} \times \{\rho_A, \rho_W\} \times \{1, 2, 3\}$ is an open set, $\bar{C}_c \cap O_c = C_c$ and $\bar{D}_c \cap O_c = D_c$, hence C_c and D_c are relatively closed sets in O_c. Here, the bar symbol on top of the sets represents its closure. F_c is a continuous, single valued function, it is locally bounded, convex and outer semicontinuous. Since D_c is closed and the jump map affects only the discrete variables, $D_c \times G_c(D_c)$ is closed as well, and the jump map is outer semicontinuous.

To analyze the stability properties of the closed-loop hybrid system $\mathscr{H}_c$, consider the following hybrid Lyapunov candidate function

$$V_c(\eta_c) = V_1(\bar{\eta}) + (\rho - \rho_d)^2 + (q - q_d)^2. \tag{31}$$

The time derivative of V_c, everywhere except in the jumps, takes the form

$$\begin{aligned} \dot{V}_c(\eta_c) &= \langle \nabla V_c(\eta_c), F_c(\eta) \rangle \\ &= \langle \nabla V_1(\bar{\eta}), F_{\bar{\xi}}(\bar{\eta}, \kappa_h(\bar{\eta}) \times q) \rangle \quad \forall\ \eta_c \in C_c. \end{aligned} \tag{32}$$

Since this is a hybrid system, evolutions on V_c may be produced by continuous dynamics or discrete jumps. To apply the hybrid LaSalle's invariance principle (Goebel et al., 2012), the boundary functions for the continuous variations u_C and for the discrete ones u_D, are computed as

$$u_C := \begin{cases} \max\limits_{\upsilon \in F_c(\eta_c)} \max\limits_{\zeta \in \nabla V_c(\eta_c)} \langle \zeta, \upsilon \rangle & \eta_c \in C_c \\ -\infty & \text{otherwise} \end{cases} \tag{33}$$

$$u_D := \begin{cases} \max\limits_{\zeta \in G_c(\eta_c)} \{V_c(\zeta) - V_c(\eta_c)\} & \eta_c \in D_c \\ -\infty & \text{otherwise} \end{cases} \tag{34}$$

Table 1
Simulation parameters.

m	V [cm^3]	$J \times 10^{-3}$[a]	$K_m \times 10^{-5}$	b
0.45	360	[4, 4, 3]	16.85	7.15
$\mathbf{C_{D_\xi}}$	$\mathbf{C_{D_\phi}}$	$\mathbf{K_{p_\xi}}$ [a]	$\mathbf{K_{d_\xi}}$ [a]	l [cm]
0.01	0.01	[1.1, 1.1, 5.5]	[3.5, 3.5, 5.9]	0.1
ϵ_1	ϵ_2	$\mathbf{K_{p_\phi}}$ [a]	$\mathbf{K_{d_\phi}}$ [a]	T_n
0.05	0.2	[6, 6, 200]	[1.1, 1.1, 20]	6

[a] Diagonal elements of the matrix.

applying a hybrid control of the form (30), satisfying $\langle \nabla V_1(\bar{\eta}), F_{\bar{\xi}}(\bar{\eta}, \kappa_h(\bar{\eta}) \times \{1, 3\}) \rangle < 0$ (see for example (15)) and choosing the transition law (22), it can be seen that $u_C = 0$ for all $\boldsymbol{\eta_c} \in C_c$. As for the discrete part

$$V_c(G_c(\eta_c)) - V_c(\eta_c) = \begin{cases} -3 & \boldsymbol{\eta_c} \in D_1 \\ -1 & \boldsymbol{\eta_c} \in D_2 \\ -(\rho_A - \rho_W)^2 & \boldsymbol{\eta_c} \in D_3 \cup D_4 \end{cases} \tag{35}$$

then the discrete bound is $u_D = -1$ for all $\boldsymbol{\eta_c} \in D_c$. According to Goebel et al. (2012, Theorem 8.2), all the solutions to the system approach the largest invariant subset of

$$V_c^{-1}(r) \cap U \cap [\overline{u_C^{-1}(0)} \cup (u_D^{-1}(0) \cap G_c(u_D^{-1}(0)))] \tag{36}$$

for some $U \subset \mathbb{R}^{14}$, $r \in \mathbb{R}$. Taking into account the constraint in the desired trajectory $|z_d| > \epsilon_2$, it follows that $u_D^{-1}(0) = G_c(u_D^{-1}(0)) = \{\emptyset\}$ and $u_C^{-1}(0) = \mathbf{0}$, where $\mathbf{0} \in C_c$ is the origin. Henceforth, the largest invariant set in (36) is the origin, and every solution to the closed-loop hybrid system (28)–(29) with control law (30) converges to the origin. It is concluded that every solution to the close-loop hybrid system is precompact, and the origin is globally asymptotically stable.

4. Simulations

In order to test the validity of the proposed control strategy, numerical simulations were carried out using *MATLAB Simulink*®. A point mass with instant changes of density when the vehicle exits the transition zone is considered. Note that this is harsher than the real case, where the density changes abruptly but taking intermediate values. A small hysteresis is introduced around the interface in order to avoid chattering. Table 1 presents the parameters used, where it is important to point out that the same control gains were applied for both modes, in air and underwater, after the corresponding density adaptation. Due to the complexity involved in the computation of the drag coefficients, the values adopted in the simulation are just intended to exemplify the effects of these forces on the system, and are set to a constant value. Unless otherwise stated, International System base units (SI) are employed. The mission consisted of (1) traveling 2 m underwater in the z-direction; (2) traveling 2 m in the y-direction followed by 2 m in the x-direction; (3) traveling in the z-direction back to the surface; (4) flying 2 m above the water level; (5) displace again 2 m in the y then x-direction and (6) return to the water. The results are shown in Fig. 7 through 9. The real and desired positions for each coordinate are shown in Fig. 7, where there are three transitions at times 0.27 s, 27.08 s and 50.80 s (solid vertical lines). The darker (blue) areas indicate when the vehicles operates underwater. The simulation proves, as expected, that dynamics underwater are slower than in air due to the damping action of the drag force, however, the inclusion of a compensation term for the drag in the control law helps to attenuate this effect. It can also be observed that fast movements in the horizontal plane may disturb the altitude due to the high coupling in their dynamics (see time 10 s and 15 s). This can lead to undesired behavior while working close to the transition zone. A possible solution would be to define one boundary ϵ_2 to enter the transition zone and another one ϵ_3 to exit it.

Fig. 8 depicts the orientation of the vehicle during the mission (top three) and the total thrust commanded to the motors (bottom). From

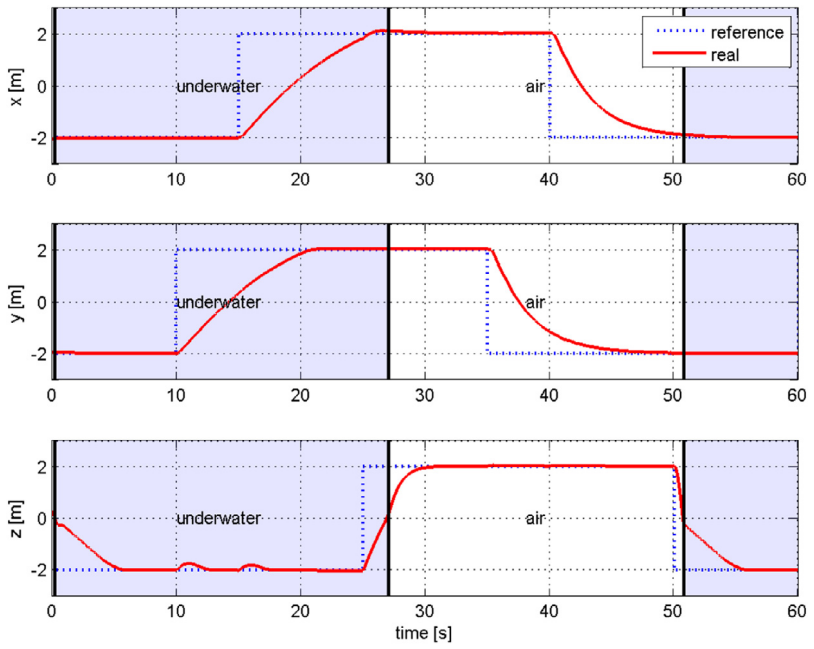

Fig. 7. x, y and z (from top to bottom) position during the mission. Three transitions take place at 0.27 s, 27.08 s and 50.80 s. The darker (blue) area highlights when the vehicle is on underwater mode, and the white area represents air mode. (For interpretation of the references to colour in this figure legend, the reader is referred to the web version of this article.)

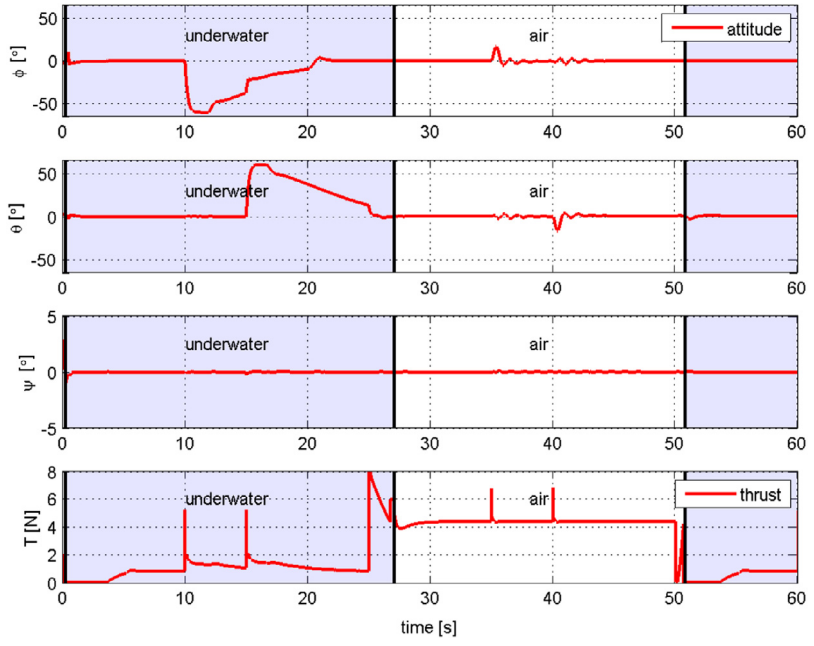

Fig. 8. Orientation response (top three) and total thrust force (bottom) underwater and in air. Underwater movements require higher angular changes to overcome drag forces.

this Figure, it can be observed that horizontal displacements underwater demand larger changes on the angles (up to 60°) due to the effect of buoyancy and the drag forces. The high coupling of the system produces a large change on the direction of the thrust force, affecting the control over z, and special attention must be paid while moving simultaneously in the three directions. The bottom plot in Fig. 8 shows the total thrust and the action of the transition controller just before each transition takes place (solid vertical lines). Observe that higher thrust is demanded in air to overcome the weight of the vehicle, while underwater the buoyancy force helps with this task, decreasing the energy consumption and allowing for higher operation time. This is one of the main advantages of this new kind of vehicles.

Finally, Fig. 9 shows the complete mission in a three dimensional (3D) representation, where the shaded (blue) volume indicates the water and the darker (green) planes represent the boundaries of the transition zone. The simulation demonstrated the good performance of the control strategy for both mediums, while handling the drastic changes in density.

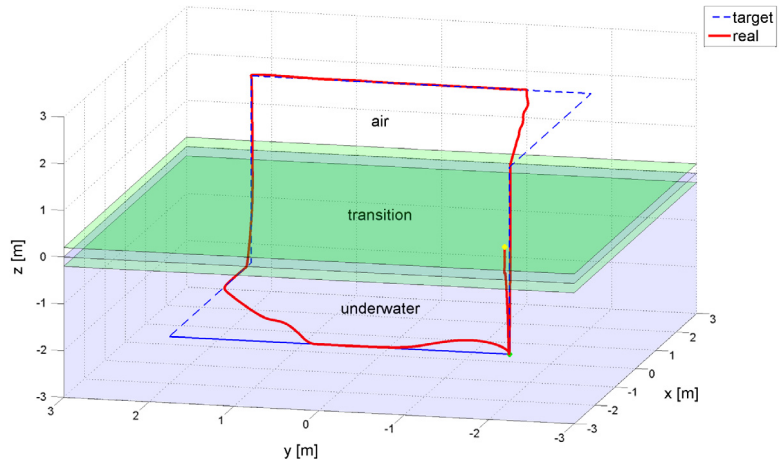

Fig. 9. 3D representation of the mission. The vehicle starts close to the water (solid yellow cross mark), submerges immediately to −2 m, moves 2 m first on y then on x, before emerging again to the air to displace 2 m on y then x and go back underwater. The darker (green) planes signal the boundaries of the transition zone, while the shaded (blue) volume represents the water. (For interpretation of the references to colour in this figure legend, the reader is referred to the web version of this article.)

5. Experimental setup: The naviator multi-medium vehicle

The experimental platform, developed as part of earlier work, relies on the simple and effective use of independently controlled rotors to compensate for situations in which the vehicle operates in both a dense fluid and sparse gas such as water and air. This condition of multi-medium operation is optimal to facilitate traversing across discrete fluid boundaries. Several concepts were considered and the robustness of multi-rotors focused the selection to a handful of such configurations, each able to adapt the use of multi-planar rotors to aid in transition. To this end, the concept presented consists of coaxial rotors allowing each thrust producing axis to operate in more than one fluid, though the rotors need not be directly in line with each other and may be offset for optimization. However, the X8 configuration (also called octa-quadcopter) was preferred because it is well studied, thus allowing the focus to remain on the innovation herein, which is of a multi-medium vehicle capable of seamless transition and operation in both air and underwater. The X8 configuration consists of eight rotors arranged in four arms, each having a pair of two coaxial counter rotating rotors (see Fig. 10). Every rotor consists of a brushless direct current (BLDC) motor and an air propeller. A BLDC electronic speed controller (ESC) commutates the motor according to Pulse Width Modulation (PWM) inputs from the autopilot. Such ESCs were modified in order to allow also lower motor's speeds required for underwater mode (between 30–350 RPM underwater for 230–6500 RPM in air). It is interesting to notice that the same propellers were used for both mediums showing comparable performance. In particular, the propeller efficiency for air is known to range from 0.2 to 0.6, while in water it was found to be around 0.3 and 0.39 (Villegas, Mishkevich, Gulak, & Diez, 2017). Power from the battery is also regulated through the battery eliminating circuit (BEC) and provided to the autopilot. The autopilot used in this platform is the ArduPilot Mega (APM) version 2.6, which comprises of accelerometers, gyroscopes, a barometer and a microcontroller.

The prototype is designed to be near to neutrally buoyant ($m \approx \rho_W V$) in order to optimize operation underwater by compensating the weight of the vehicle, while a small negative buoyancy ($m > \rho_W V$) is selected in order to add a negative vertical force component to ensure transition between mediums and downwards navigation underwater.

Although the vehicle is able to communicate wirelessly for a few feet while submerged using standard radio frequency equipment, the presented vehicle uses a tether to prevent signal interruption and to allow for faster data rates, which is important for observing real time experimental data during field tests. In a real scenario, a combination of radio frequency and acoustics will be utilized. The 30 m tether consists of a one way pulse-position modulation (PPM) signal, a two-way telemetry link and ground for a total of four wires. The tether attaches to a buoy that then transmits/receives the data wirelessly to/from the ground station. The buoy is meant to increase the lateral range of the vehicle beyond that of the tether by having the vehicle tow it as needed, allowing the vehicle to operate freely in a large body of water. The water-sensitive components of the vehicle are contained within a waterproof pressure vessel. An overview of the system is shown in Fig. 11.

Fig. 10. Naviator NV05b, Unmanned aerial/underwater vehicle in a X8 configuration during an outdoor ocean flight test, 2016.

This standard configuration is supplemented by an external pressure sensor and a set of two water sensors, which are placed on the outer bound of the top rotor plane and bottom rotor plane. The pressure sensor is placed near the mid-plane of the water sensor planes. Furthermore, due to its unique application, both the autopilot and ESCs employ custom firmware, allowing for smooth underwater operation and different control schemes.

A video showing the capability of the experimental platform to smoothly transition between mediums is available in the supplementary material (see Video 1).

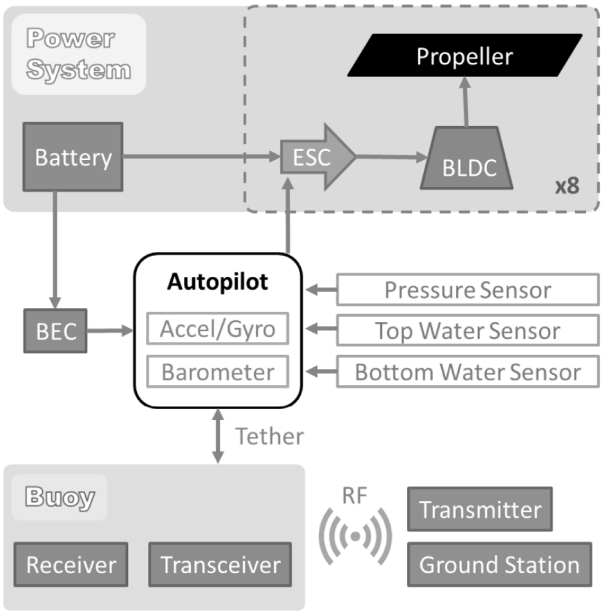

Fig. 11. An overview of the Naviator vehicle platform.

6. Preliminary real-time experiments

The experimental platform described in the previous section was tested in real-time experiments to analyze the performance of the vehicle in air and underwater, in semi-autonomous mode, where the orientation and altitude are controlled automatically by PID controllers with compensation of the restoring forces, i.e. the control law used in the experiment $u = [\nu_e \ \Gamma_e]$ is given by

$$\nu_e = (g(m - \rho V) - k_{pz}\bar{z} - k_{dz}\dot{\bar{z}} - k_{iz}\int \bar{z}dt)e_3 \tag{37}$$

$$\Gamma_e = -\mathbf{K}_{\mathbf{p}_\phi}(\Phi_1 - \Phi_p) - (\mathbf{K}_{\mathbf{d}_\phi})\Phi_2 \tag{38}$$

where k_{pz}, k_{dz} and k_{iz} are positive control gains and Φ_p is the desired orientation commanded by the human pilot. Control on the x and y coordinates is done manually due to the lack of a precise estimation of the vehicle's position. Precise localization for an air/underwater vehicle is an interesting problem without a straightforward solution since GPS signals are not available underwater and acoustic sensors normally used for underwater localization are too heavy to be carried on flight by a small vehicle. Hence, only performance on altitude is tested for both media (air and water), along with the transition between them. The transition-in strategy consists in switching off the motors once the water sensor on the bottom is triggered. The physical parameters of the multi-medium vehicle are summarized in Table 2. Experimental drag coefficients are currently not available due to the lack of reliable sensors for both mediums. One of the main advantages of the proposed configuration with respect to traditional underwater vehicles arises as a direct consequence of the lightweight requirement in air. A reduced weight allows to decrease the buoyancy and therefore the volume of the vehicle, resulting in smaller added mass and added moments of inertia.

The mission consists of: holding a reference altitude of 2.5 m for 15 s by means of an altitude controller; slowly descending at a rate of 10 cm/s; transitioning into the water and descending with rotors off until approaching the new depth reference of −0.5 m; and activating the altitude controller to maintain depth for 15 s. The performance of the altitude controller during the experiment is depicted in Fig. 12. It can be seen that the same vehicle is perfectly capable of evolving in both media and maintain its altitude. However, performance in air mode is affected by measurement noise, where is important to notice

Table 2
Experimental parameters.

m	V [cm^3]	$J \times 10^{-3}$ [a]	$K_m \times 10^{-5}$
3.85	3630	[69.01, 69.24, 118.96]	8.49
ϵ_1	ϵ_2	l	T_n[%]
0.153	0.204	0.27	50–65.7
$\mathbf{K}_{\mathbf{p}_\phi}$ [a]	$\mathbf{K}_{\mathbf{d}_\phi}$ [a]	$\mathbf{K}_{\mathbf{p}_z}$	$\mathbf{K}_{\mathbf{d}_z}$
[0.25, 0.25, 0.30]	[0.002, 0.002, 0]	$\{air : 1, water : 5\}$	0
m_a [b]	$J_a \times 10^{-3}$ [c]	r_v	
0.536	1.441	0.0635	

[a] Diagonal elements of the matrix.

[b] Approximation for underwater operation, considering the pressure vessel as the main volume to be moved, with a spherical shape of radius $r_v = 0.0635$ m.

[c] Approximation around each axis for underwater operation, considering the pressure vessel as a thin spherical shape of radius $r_v = 0.0635$ m.

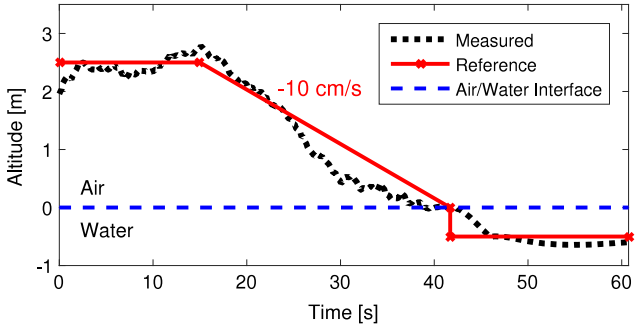

Fig. 12. Real-time experiment on altitude. The vehicle hovers at an altitude of 2.5 m for 15 s, descends at a rate of 10 cm/s until it reaches the water level, transitions into the water, then it sinks until it approaches the depth reference of 0.5 m and maintains the desired depth for 15 s.

that the same pressure sensor is used for altitude measurements in both mediums, with an accuracy within one centimeter underwater and half a meter in air. The observed error in altitude hold during time 25 s–40 s is attributed to the increased measurement error of the pressure sensor while in air. The throttle percentage is presented in Fig. 13, where it can be appreciated when the transition mode is triggered (motors off) as soon as the water sensor is activated, in time 42 s–45 s. It is also interesting to notice the vast difference in throttle required for altitude hold in air versus maintaining depth underwater, mainly due to the increase in the buoyancy force associated with the change of density. Finally, Fig. 14 shows the orientation of the vehicle during the mission. Observe that the attitude controller satisfactorily stabilize the vehicle's orientation for hover in air and underwater. The small perturbations observed are produced by manual commands from the pilot to correct for horizontal displacements. Also note that during the transition (42 s–45 s) the orientation error is slightly increased, but once the vehicle goes out of the transition mode, it is able to recover and regain proper orientation.

A video of the experiment into the water described in this section is provided as supplementary material (see Video 2).

A transition-out strategy was also conducted. The mission consists of: starting 1 m underwater; proceeding to a reference depth of −0.5m; going to a reference depth of 0 m; switching to transition-out mode; and maintaining a 0.5m reference. The transition-out mode applies the transition-out strategy where when the top water sensor registers water, the vehicle switches the rotors to air mode such that throughout the entire process, the throttle ensures a thrust T_n, as discussed in Section 3.2, that is capable of bringing the vehicle out of the water. The altitude/depth during the mission as measured by the vehicle is shown in Fig. 15. It can be seen that while underwater, the vehicle converges to the desired reference very well, but with a slight offset. The offset

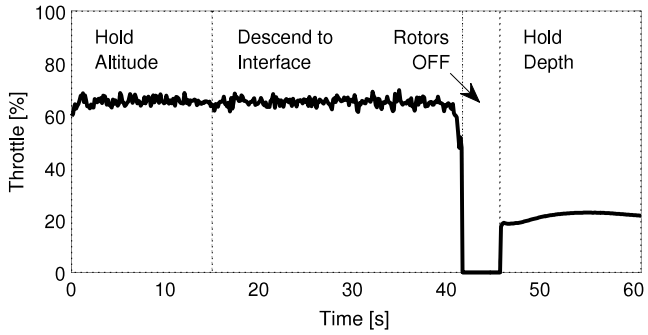

Fig. 13. Throttle percentage output during the autonomous mission into water.

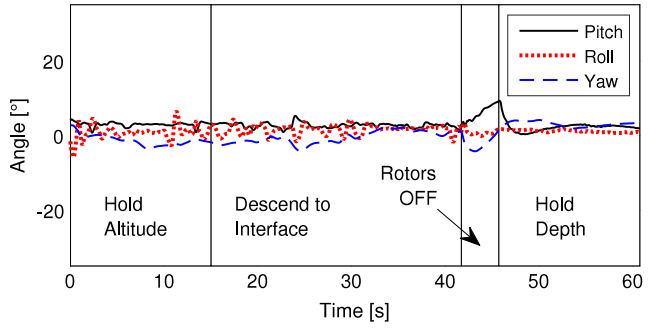

Fig. 14. Orientation during the experiment into the water.

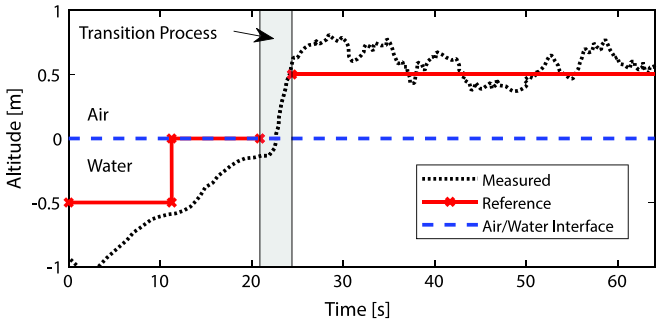

Fig. 15. Real-time experiment on altitude. The vehicle starts 1 m underwater, goes to 0.5 m, goes to 0 m, proceeds to transition out of the water, and goes to a reference of 0.5 m.

can be attributed to the weight of the tether, which is not compensated for. The transition mode is shown by the shaded region and successfully brings the vehicle out of the water. However, once the vehicle exits the transition mode to hold altitude, it is observed that the altitude is mostly higher than the desired reference. The throttle for the mission out of the water is given in Fig. 16. The regions 0 s–12 s and 12 s–21 s show a typical step response for the depth PID controller going to the −0.5 m and 0 m targets, respectively. The transition period between 21 s and 24 s shows that the throttle that is provided ensures that the overall thrust produced is sufficient to compensate for the restoring forces, at all times during transition out. Finally, after the transition mode, the output throttle ensures that the vehicle maintains its altitude in the air. Throughout this experiment, which focuses on the transition of the vehicle, the altitude was controlled autonomously by the vehicle autopilot according to the desired references, but the position was controlled using manual inputs of roll, pitch and yaw. The resulting Euler angles corresponding to the orientation of the vehicle during the mission are shown in Fig. 17, which shows that although the majority

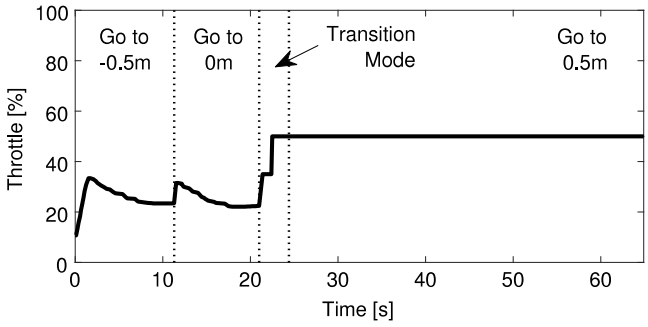

Fig. 16. Throttle percentage output during the autonomous mission out of water.

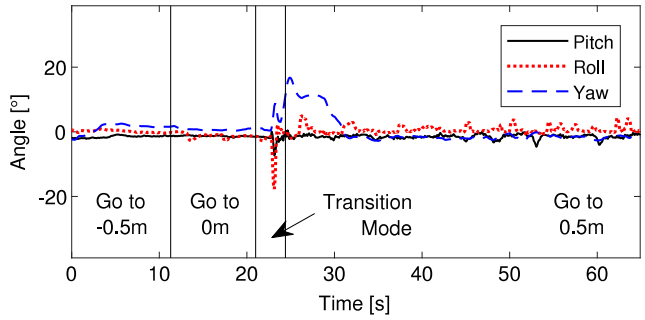

Fig. 17. Orientation during the experiment out of the water.

of the mission yielded small angle variations, the transition mode had an adverse effect on both roll and yaw. This is because the mission investigated a jump from water mode (low RPM) to air mode (high RPM) triggered by the vehicle water sensors and since the rotor response times vary slightly, such a jump caused a perturbation in the attitude of the vehicle, which was quickly corrected by the angle and torque controllers once all rotors were up to speed. These perturbations can be reduced by gradually increasing throttle from low RPM to high RPM. However, this experiment demonstrates that even without a smooth ramping up of the rotor angular velocities, the vehicle is still capable of traversing out of the water.

A video of the experiment out of the water described in this section is provided as supplementary material (see Video 3).

7. Perspectives and future work

The problem of autonomous navigation and control for an unmanned multi-medium vehicle was studied in this work, and a mathematical model was proposed as a hybrid system with discrete events and continuous time dynamics. The continuous dynamics were obtained using the Newton–Euler formalism for both cases, in air and underwater. The discrete events model the drastic change on the medium density as well as the switching between the control laws.

First, considering that a reliable estimation of the vehicle's position is available, a trajectory tracking strategy was designed for the system with constant density, using the desired angles as virtual control inputs for the position control, along with a control technique based on feedback linearization. Then, a transition strategy was developed to handle the change between the two mediums. Moreover, a closed-loop hybrid system was provided to represent the full system. The stability of the hybrid closed-loop system was analyzed using the hybrid variations of the Lyapunov method and invariance principle, including the stability during the transition. The performance of the control system was studied through simulations.

Furthermore, an experimental setup was successfully developed and some preliminary results were introduced for altitude control with air-to-water and water-to-air transition. To the authors knowledge, this is the first multirotor vehicle equally adept to operating underwater and in air, as shown by the real-time experiments.

Design and control of multi-medium vehicles arises as an exciting new research area, with a wide range of possibilities for future work. For example, it is important to add robustness against uncertainties and external perturbations, present in natural conditions (wind and water currents). Also, the already available experimental platform may be used to adapt and test other kinds of control strategies, and the control design can be extended to the actuators. Moreover, model validation and parameter identification remain open for future work.

Still, the main challenge for autonomous navigation of air/water vehicles, besides the communication problem underwater, is the lack of a good position estimation, specially underwater were GPS signals are not available, and underwater localization systems are not optimized, in terms of weight and size, for flight operation. Depending on the application, some considered solutions are inertial navigation, acoustic solutions and computer vision.

Acknowledgment

This work was supported by Office of Naval Research (ONR), Grant No. N00014-15-2235 with Dr. Thomas McKenna serving as Program Manager.

Appendix A. Supplementary data

Supplementary material related to this article can be found online at https://doi.org/10.1016/j.conengprac.2018.04.006.

References

Alexis, K., Huerzeler, C., & Siegwart, R. (2014). Hybrid predictive control of a coaxial aerial robot for physical interaction through contact. *Control Engineering and Practice*, *32*, 96–112.

Bertrand, S., Guénard, N., Hamel, T., Piet-Lahanier, H., & Eck, L. (2011). A hierachical controller for miniature VTOL UAVs: Desing and stability analysis using singular perturbation theory. *Control Engineering Practice*, *19*, 1099–1108.

Cassau, P., Sanfelice, R., Cunha, R., Cabecinhas, D., & Silvestre, C. (2015). Robust global trajectory tracking for a class of underactuated vehicles. *Automatica*.

Castillo, P., Lozano, R., & Dzul, A. (2005). *Modelling and control of mini-flying machines*. Londres: Springer-Verlag.

Crespi, A., Karakasiliotis, K., Guignard, A., & Ijspeert, J. (2013). Salamandra robotica II: an amphibious robot to study salamander-like swimming and walking gaits. *IEEE Transactions on Robotics*, *29*(2), 308–320.

Drews Jr., P., Neto, A., & Campos, M. (2014). Hybrid unmanned aerial underwater vehicle: Modeling and simulation. In *International conference on intelligent robots and systems, IROS*.

Edwards, D. (2014). Flimmer: a flying submarine. *Naval Research Laboratory Spectra*, 6–9.

Fabian, A., Feng, Y., Swartz, E., Thurmer, D., & Wang, R. (2012). Hybrid aerial underwater vehicle (MIT Lincoln Lab) SCOPE projects.

Fossen, T. (1994). *Guidance and control of ocean vehicles*. England: John Wiley and Sons.

Goebel, R., Sanfelice, R., & Teel, A. (2012). *Hybrid dynamical systems: Modeling, stability and robustness*. Princeton University Press.

Hamel, T., Mahony, R., Lozano, R., & Ostrowsky, J. (2002). Dynamic modeling and configuration stabilization for a X4-Flyer. In *15th triennial IFAC world congress*.

Jones, K., Dobrokhodov, V., & Dillard, C. (2016). Aqua-quad — solar powered, long endurance, hybrid mobile vehicle for persistent surface and underwater reconnaissance, Part I — Platform design. In *OCEANS 2016 MTS/IEEE*.

Kendoul, F., Lara, D., Fantoni, I., & Lozano, R. (2006). Nonlinear control for systems with bounded inputs: real-time embedded control applied to UAVs. In *Proceedings of the 45th IEEE conference on decision and control*.

Kollmorgen, (2009). *Sea sentry organic submarine launched UAV*. Radford: Kollmorgen Corporation.

Kundu, P., & Cohen, I. (2008). *Fluid mechanics* (4th Ed.). (pp. 368–376). USA: Elsevier Science, ch. 10.

Maia, M.M., Soni, P., & Diez, F.J. (2015). Demonstration of an aerial and submersible vehicle capable of flight and underwater navigation with seamless air-water transition. arXiv preprint arXiv:1507.01932.

Majumdar, D. (2013). U.S. Navy launches UAV from a submarine. U.S. Naval Institute News.

Mercado, D., Castillo, P., Castro, R., & Lozano, R. (2014). 2-sliding mode trajectory tracking control and EKF estimation for quadrotors. In *The 19th IFAC world conference*.

Naldi, R., Furci, M., Sanfelice, R., & Marconi, L. (2013). Global trajectory tracking for underactuated VTOL aerial vehicles using a cascade control paradigm. In *52nd IEEE conference on decision and control*.

Neto, A., Mozelli, L., Drews Jr., P., & Campos, M. (2016). Attitude control for an hybrid unmanned aerial underwater vehicle: a rubust switched strategy with global stability. In *International conference on robotics and automation, ICRA*.

Petrov, G. (1995). Flying submarine. *Journal of Fleet*.

Ranganathan, T., Thondiyath, A., & Kumar, S. (2015). *Design and analysis of an underwater quadrotor — AQUAD underwater technology (UT)*. Chennai, India: IEEE.

Roskam, J. (1982). *Airplane flight dynamics and automatic flight controls*. (pp. 25–31). Roskam Aviation and Engineering Corporation, ch. 2.

Smith, D., & Sanfelice, R. (2016). Autonomous waypoint transitioning and loitering for unmanned aerial vehicles via hybrid control. In *AIAA guidance, navigation and control conference*.

Tanaka, T., Fuji, H., Matsuo, T., & Takimoto, T. (2016). Development of quad-rotor type underwater robot for fixed-point observation. In *Autonomous underwater vehicles, AUV*. Tokio, Japan: IEEE/OES.

Unknown, (1930). Denmark amazing submarine plane. *Modern Mechanics and Inventions*, *25*, 74–75.

van der Shaft, A., & Schumacher, J. (2000). *An introduction to hybrid dynamical systems*. Springer.

Villegas, A., Mishkevich, V., Gulak, Y., & Diez, F. J. (2017). Analysis of key elements to evaluate the performance of a multirotor unmanned aerial–aquatic vehicle. *Aerospace Science and Technology*, *70*, 412–418.